INTERNATIONAL JOURNAL OF CLIMATOLOGY
Int. J. Climatol. **33**: 2846–2854 (2013)
Published online 11 December 2012 in Wiley Online Library
(wileyonlinelibrary.com) DOI: 10.1002/joc.3634

RMetS
Royal Meteorological Society

Seasonal prediction of accumulated tropical cyclone kinetic energy around Taiwan and the sources of the predictability

Mong-Ming Lu,[a] Ching-Teng Lee[a] and Bin Wang[b]
[a] *Research and Development Center, Central Weather Bureau, Taipei, Taiwan R.O.C.*
[b] *Department of Meteorology, School of Ocean and Earth Science and Technology, University of Hawaii at Manoa, Honolulu, HI, USA*

ABSTRACT: Tropical cyclone (TC) is the most hazardous high-impact weather system in Taiwan. TC seasonal prediction affecting the Taiwan area is extremely challenging because of the relatively small target area and highly variable TC genesis locations and tracks. This paper presents an empirical seasonal forecast model for predicting TC activity around Taiwan during the peak season (June through September). The predictand is the accumulative cyclone kinetic energy (ACE) of the invading TCs within the 'influence domain' defined as an area extending 300 km away from the coast. The predictors consist of the sea surface temperatures (SSTs) and their tendency over the tropical Indo-Pacific Ocean and the sea level pressure (SLP) over extratropical East Asia during the spring season. The source of the predictability is rooted in the spring to summer evolution of the monsoon subtropical high-ENSO system in association with the evolution of the Indo-Pacific SST anomalies. When the spring SST anomaly is warm over equatorial western Pacific, while it is cold but with a warming tendency over tropical South Indian Ocean, the coupled atmospheric and oceanic anomalies evolve into a favourable large scale condition conducive for active typhoon occurrence in the Taiwan area during the ensuing summer. The empirical prediction model presented in this paper has important implications for predicting TCs affecting a much larger area covering southeast China and the East China Sea ($r = 0.97$).

KEY WORDS tropical cyclone; seasonal prediction; monsoon-ENSO evolution; accumulative cyclone kinetic energy

Received 15 March 2012; Revised 5 September 2012; Accepted 28 October 2012

1. Introduction

Taiwan is located in a tropical cyclone (TC) prone area of the subtropical western North Pacific (WNP). The leaf-shaped island extends 394 km NNE–SSW and 144 km ESE–WNW with a coastline of 1566 km. The population is more than 23 million. Although the area is small, the island on average can be hit by 3–4 TCs a year, which means that about 12–16% of the TCs formed in the WNP can hit Taiwan. The prediction of such extreme events with small probability is extremely challenging.

Various forecast models have been developed for specific TC prone areas in East Asia such as Taiwan (Lu *et al.*, 2010, Chu *et al.*, 2007; Chu *et al.*, 2010), Korea (Choi *et al.*, 2009), Japan (Goh and Chan, 2012), the East China Sea (Kim *et al.*, 2010), and South China (Liu and Chan, 2003). Recently, there are seasonal forecast models developed for the Southern Hemisphere as well (e.g. Liu and Chan, 2010; Werner and Holbrook, 2011). The WNP TC activity is known to possess several kinds of variations that differ in their time scales. The interannual variations are affected by the sea surface temperatures (SSTs) anomalies over the Pacific such as ENSO (Chan 1985, 2000; Chan *et al.*, 1998; Wang and Chan, 2002; Camargo *et al.*, 2007a; Goh and Chan, 2012) and over the Indian Ocean (IO) (Du *et al.*, 2011; Zhan *et al.*, 2011), the biennial variations are related to stratospheric quasi-biennial oscillation (Chan, 1985), and the interdecadal variations are related to Pacific Decadal Oscillation (Ho *et al.*, 2004) and the Antarctic Oscillation (Ho *et al.*, 2005).

The predictability of TC frequency in a limited area relies on factors that control TC trajectories. Over the WNP region influential large-scale features in the low-level include the western Pacific subtropical anticyclone and monsoonal flow (Harr and Elsberry, 1995; Kuo *et al.*, 2001; Liu and Chan, 2002), and in the upper-level tropical upper-tropospheric troughs (TUTTs) (Sadler, 1978; Montgomery and Farrell, 1993). Camargo *et al.* (2007b, 2007c) found that WNP TC trajectories can be grouped into seven clusters. The clusters are sensitive to both genesis location and trajectory patterns. Three of the clusters are ENSO related (Camargo *et al.*, 2007c). During El Niño years, the preferable location of TC genesis shifts southeastward, while during La Niña years the preferable location shifts northwestward. The type of highly populated cluster, wherein more recurving trajectories are observed, tends to occur more often during La Niña years. Kim *et al.* (2011) found three different ENSO regimes with distinctly different influences on Pacific TCs. In the east Pacific warming

* Correspondence to: Mong-Ming Lu, Research and Development Center, Central Weather Bureau, No.64, Gongyuan Road, Taipei City 10048, Taiwan R.O.C.
E-mail: lu@rdc.cwb.gov.tw

(EPW) years, the genesis and the track density of TCs tends to be enhanced over the southeastern part and suppressed in the northwestern part of the western Pacific. In the central Pacific warming (CPW) years, the TC activity is shifted to the west and is extended through the northwestern part of the western Pacific. The westward shifting of CPW-induced heating and monsoon trough intensification provides a more favourable condition for TC landfall but suppressing condition for TC activity in the eastern Pacific basin. In the east Pacific cooling (EPC) years, almost a mirror image of the EPW relationship is found between the variables.

Motivated by the IO capacitor mechanism proposed by Xie *et al.* (2009), Zhan *et al.* (2011) found the anomalous summer SSTs over eastern IO (10°S–22.5°N, 75°–100°E) show different influence mechanisms on the TC activity over WNP than ENSO. The WNP TC activity is more active during the cold years of eastern IO SST and less active during the warm years. The influence is through the modulation of the western Pacific monsoon trough and atmospheric Kelvin wave activities by the IO SSTs. Different from the proposed capacitor mechanism, which emphasizes more on the SST over the east tropical and northern IO, a number of studies (Terray *et al.*, 2005; Terray *et al.*, 2007; Yoo *et al.*, 2006; Kim *et al.*, 2012) proposed that the southern (south of 10°S) IO SST anomalies have stronger influence on the Asian summer monsoon than its northern (north of 10°N) IO counterpart. The springtime SST variations over the southern IO lead to opposite changes over the Indian and western Pacific monsoon regions in ensuing summer, reinforcing the out-of-phase relationship that appears often between two monsoon components (Yoo *et al.*, 2006). Warmer than normal SST over the southeastern IO tends to enhance the Indian monsoon rainfall, while weakening the monsoon rainfall over the western Pacific trough climatological location.

In light of recent findings, this paper expands the previous studies (Lu *et al.*, 2010; Chu *et al.*, 2007; Chu *et al.*, 2010) by including the IO and continental Asia when searching for predictors. A much broader domain (30°S–60°N, 40°E–100°W) than before (10°S–30°N, 110°E–170°W) is used in this study. A broader domain is necessary for developing a seasonal forecast model with sound physical basis.

The definition of influence-Taiwan TCs is also different from previous studies. In this paper the TC influence domain is defined as the area expanded from Taiwan's coastline outward by 300 km on a 0.1° × 0.1° of latitude and longitude mesh (Figure 1). The area has a different shape and is slightly larger than the previously used rectangular box area of 21°N–26°N and 119°E–125°E (Lu *et al.*, 2010; Chu *et al.*, 2007; Chu *et al.*, 2010). The old definition gives heavy weights to TCs east of Taiwan but undermines the influence of TCs from the south and southwest. The track density map (Figure 1) shows that the new domain includes three major centres of occurrence located near (22°N, 118°E), (21°N, 121°E), and (22°N, 123°E), but the rectangular box does not include the centre near (22°N, 118°E). The rectangular box extends too much to the southeast so that some tracks reflecting the favourable path of TCs that travel from the Philippine Sea northward toward Japan can be falsely treated as affecting Taiwan. Figure 2 shows the tracks of all Taiwan TCs during July–September from 1970–2007 and the locations of the associated first recorded TCs. The TCs that affect Taiwan are primarily from three directions: S–SW, SE, and E. Most S–SW TCs are formed over the SCS, while the E or SE TCs are formed over the Philippine Sea.

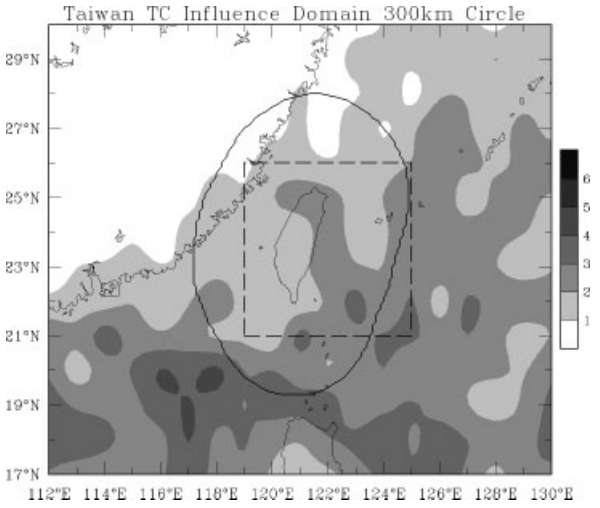

Figure 1. The areas (solid and dashed lines) used for defining the affecting Taiwan TCs and the numbers of TCs occurred during the period of 1970–2011 counted in a 1° × 1° grid system. The solid curve shows the boundary determined by extending Taiwan's coastline outward by approximate 300 km on a 0.1° × 0.1° mesh of longitudes and latitudes. The boundary is used for defining affecting Taiwan TCs in the present study. The affecting duration is defined as from the accumulated hours from the first record to the last record of a TC within and at the boundary. The dashed line marked the area of 21°N–26°N and 119°E–125°E which is the boundary used in previous studies (Chu *et al.*, 2007; Lu *et al.*, 2010).

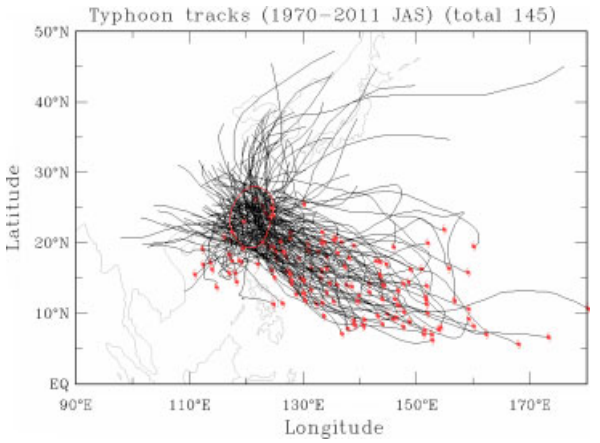

Figure 2. The tracks of all affecting Taiwan TCs during JAS of 1970–2011. The domain used for identifying the TCs is marked by the circle surrounding Taiwan.

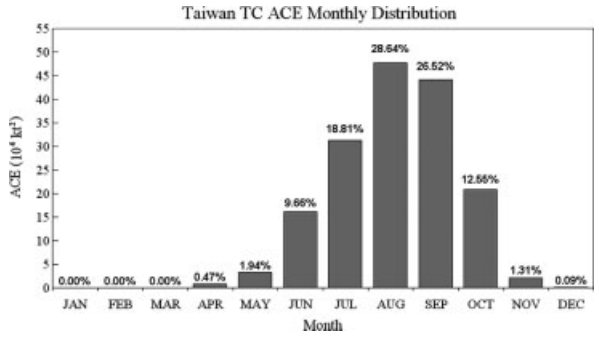

Figure 3. The 1970–2011 climate mean monthly ACE of the affecting Taiwan tropical cyclones and its percentage with relative to the annual total ACE.

The predictand of the aforementioned previous studies is the typhoon count. Although the number of typhoons is easier for the general public to understand, it is insufficient in representing the degree of impact by these TCs and the economic loss caused by typhoon disasters. The degree of TC impact is determined by the TC number, the resident time and intensity in the influence domain. For this reason, the *a*ccumulative *c*yclone kinetic *e*nergy (ACE) is chosen as the predictand in this study, because the ACE provides integrated information about the number, intensity, and the duration of TCs stay in the vicinity of Taiwan. The correlation of the annual ACE and economic loss from TCs is 0.39 which is significant at the level of 0.1, but, the TC count and economic loss correlation (0.25) is not significant at the same level.

The ACE definition is the same as the ACE issued in NOAA's seasonal hurricane outlook for the Atlantic and eastern North Pacific regions and it is the sum of the squares of the maximum sustained surface wind speed (knots) measured every 6 h when the TC is within the influence domain. The TC is required to be a named system, of which the intensity must reach at least tropical storm strength (wind speed $\geq$34 kt h^{-1}) during the storm's entire lifetime. The ACE seasonal distribution (Figure 3) suggests that almost 84% of the 'invading' TCs occurring during the peak season from June to September (JJAS). October is not included in the time period of the predictand, because the major TC activity influential factors before and after the active phase of the Indian summer monsoon season are different. The ACEs during JJA and SON are not correlated. Therefore, the predictand used in this paper is the accumulated ACE during JJAS denoted as ACE-JJAS. The ACE-SON forecast model will be presented in a separate paper.

2. Data and method

2.1. Data

The JTWC best-track dataset (Chu *et al.*, 2002), available at 6-hourly sampling frequency over the period of 1970–2011, obtained from Joint Typhoon Warning Center website (http://metocph.nmci.navy.mil/jtwc/best_tracks/), was used to calculate the ACE. TC refers to tropical storms and typhoons, which has a maximum sustained surface wind speed of 33 m s^{-1} or higher.

Several standard datasets are used to analyze the large-scale environment associated with TCs. The monthly variables, mean sea level pressure (SLP), wind at 850-, 500-, and 200-hPa levels, relative vorticity at the 850- and 700-hPa level, and total precipitable water over the WNP (0°–30°N), are derived from the NCEP-NCAR reanalysis dataset (Kalnay *et al.*, 1996). The monthly mean SSTs, at 2° horizontal resolution, are taken from the extended reconstructed SST (ERSST) dataset prepared by the National Climate Data Center (NCDC) and downloaded from the NOAA Physical System Division of the Earth System Research Laboratory in Boulder website (http://www.cdc.noaa.gov/). Only large-scale environmental parameters for the months of March, April, and May are derived as predictors.

2.2. Predictor selection and forecast experiment

The predictand presented in this paper is the ACE-JJAS of TCs invading Taiwan (hereafter the predictand is represented by ACE-JJAS for brevity). The predictors were selected using a two-step correlation analysis procedure. The first step is to calculate the correlation maps between ACE-JJAS and the large-scale environment variables in the 40°E–120°W and 30°S–50°N domain. The areas with high coherent correlations are selected. The area means of the variables and their derivatives are chosen as the predictor candidates.

In order to avoid the artificial skill due to predictor screening (DelSole and Shukla, 2009), we did not use the data after the forecast time when selecting the predictors. The data during 1970–2000 is set for predictor selection and 2001–2011 is for forecast experiment that mimics the real forecasts but runs retrospectively. In addition to the forecast experiment, we also carry out the standard cross-validation procedures for assessing the overall forecast skill during 1970–2011.

Four large-scale variables, SLP, SSTs, 500-hPa zonal wind (U500), and relative vorticity (VR500), are examined. The correlations maps between ACE-JJAS and March–May seasonal means of these four variables are presented in Figure 4. Figure 4(a) shows a large positive correlation over the equatorial western Pacific from 10°S to 10°N and 150°E to 170°E. The positive correlation east to the dateline over the subtropical eastern North Pacific from 10°N to 20°N is also significant. Another area with significant positive correlation is over the mid-latitude eastern North Pacific from 40°N to 50°N. In between two areas with large positive correlation is the negative correlation from 20°N to 30°N. Over the southern IO, we find significant negative correlation around 15°S, 100°E. To the east of Australia we find another negative area extending from the Tasman Sea to the Coral Sea.

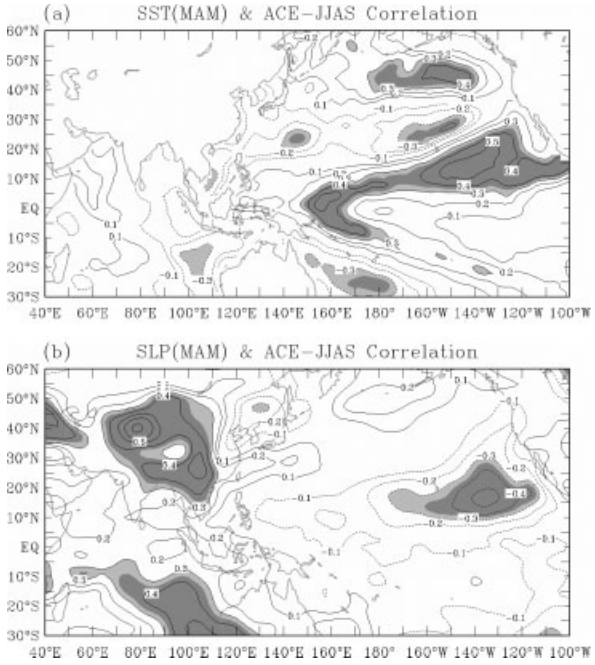

Figure 4. The linear correlation for the period of 1970–2000 between ACE-JJAS and spring seasonally averaged (March–May) (a) SST and (b) SLP. The correlations significant at the level of 0.10 (0.05) are light (dark) shaded.

In contrast to the correlation map of SST, Figure 4(b) shows that significant correlations between the SLP and ACE-JJAS are found mainly over the higher latitudes of the Eurasian continent and South IO. The positive centre appears over continental Asia and a negative centre over Northeast Asia around the boarder of China and Russia. Over the southern IO a large area of significant positive correlations occurs in a southeast–northwest orientation from Australia to the tropical western IO. The negative correlation over the subtropical Eastern Pacific corresponds well to the positive correlation in SST.

According to the seasonal correlation maps and our understanding of the physical linkage between the predictand and predictor fields, we selected 17 predictor candidates listed in Table 1 to form a predictor pool. The potential predictors are further selected through a stepwise multivariate regression procedure available in MATLAB. Given the sample size of 42, selection of four predictors seems appropriate (the ratio of predictor and sample size is about 10%) in order to avoid overfitting. The first four predictors selected as a result of F-test are SST_CIO_05-04, SLP_CN_MAM, SST_SIO_MAM, SST_WP_MAM (Table 1) in terms of the order of selection. The F-value of the regression model can pass the 90% (99%) confidence interval when four (two) predictors are used. The multiple regression correlation between ACE-JJAS and four predictors is 0.79.

3. Forecast results and skill evaluation

The overall forecast ability of the multivariate regression model can be evaluated using the standard leave-one-out cross validation (LOOCV) procedure (Lu *et al.*, 2010). The predictor and predictand data set of T time points are divided into L segments. A model is then developed using the data of $L - 1$ segments and used to predict ACE-JJAS in the remaining segment. This process is repeated by changing the segment that has been excluded from the model development. In addition to the LOOCV, we also used leave-seven-out and leave-nine-out to evaluate the forecast skill, in which the prediction target is the fourth (fifth) year of the removed consecutive seven (nine) years. Both results are similar to LOOCV. Here we will present the result for N predictions obtained from the LOOCV.

The LOOCV result of the four-predictor (SST_CIO_05-04, SLP_CN_MAM, SST_SIO_MAM, SST_WP_MAM) forecast model is presented in Figure 5. The correlation coefficient skill of the observed and LOOCV result reaches 0.52. For a sample size of 42, the critical value of 95% confidence level is 0.3 when a two-tailed t-test is applied. Using the random number re-sampling technique to resample the data sets (Chu *et al.*, 2007), the 95% (99%) confidence level is 0.26 (0.36). Accordingly, the correlation coefficient (0.52) from the model developed in this study is deemed to be skilful relative to the benchmark random samples.

To gain further insight about the prediction skill, both the observed and forecasted ACE-JJAS are grouped into tercile classes. A 3×3 verification contingency table for the observation and forecast is presented on the upper left corner of Figure 5. The highest numbers appear at the upper-left and lower-right corners, which correspond to the correct forecast for the above and below normal categories. The threshold values for the tercile categories are determined according to the climatology of 1981–2010. The 30 year period is the standard climatology recommended by WMO for weather and climate services. The Heidke skill score that is based on the hit rate as the accuracy measure is 0.39. Note that forecasts equivalent to the reference forecasts receive Heidke score of 0 (Wilks, 2006). Thus, the presented ACE-JJAS forecasts are better than the reference forecasts.

The above cross-validation may overestimate the forecast skill, because during the model development period (1970–2000) all data are included when calculating the correlation between ACE-JJAS and the large-scale variables. The retrospective forecast results from 2001–2011 (Figure 5) show good forecasts in 2001, 2003, 2005, 2006, and 2007, but not good in the last 4 years from 2008–2011. The model fails to capture the unusually high ACE in 2008 and the low ACE during the past 3 years (2009–2011). However, the model is able to capture the tendency of more active typhoon activity in the

Table 1. Predictor candidates used for forecast model development. The climatology used for anomaly calculation is the time mean of the 1970–2000 training period.

Predictor	Variables	Description
SST_WP_MAM	SST	SST anomaly over Pacific (10°S–10°N, 140°E–170°E)
SST_SIO_MAM	SST	SST anomaly over southeastern IO (25°S–10°S, 90°E–110°E)
SST_TCS_MAM	SST	SST anomaly over South Pacific (30°S–20°S, 155°E–170°W)
SST_EEP_MAM	SST	SST anomaly over equatorial eastern Pacific (10°N–22.5°N, 160°W–120°W)
SST_ECP_MAM	SST	SST anomaly over eastern central Pacific (10°N–22.5°N, 175°W–140°W)
SST_ENP_MAM	SST	SST anomaly over eastern north Pacific (35°N–52.5°N, 170°E–130°W)
SST_CIO_05-04	SST	SST tendency (May minus April) over equatorial central IO (15°S–5°N, 60°E–90°E)
SST_CIO_05-03	SST	SST tendency (May minus March) over equatorial central IO (15°S–5°N, 60°E–90°E)
SST_EEP_05-04	SST	SST tendency (May minus April) over equatorial eastern Pacific (12.5°S–0°S, 160°W–120°W)
SST_ESP_05-04	SST	SST tendency (May minus April) over eastern south Pacific (30°S–15°S, 160°W–120°W)
SST_TCS_05-04	SST	SST tendency (May minus April) over south Pacific (30°S–15°S, 150°E–175°W)
SLP_CN_MAM	SLP	SLP anomaly over East Asia (35°N–50°N, 117.5°E–140°E)
SLP_EQ_05-04	SLP	SLP tendency (May minus April) over Pacific (20°S–15°N, 140°E–160°W)
SLP_SIO_MAM	SLP	SLP anomaly over southeastern IO (25°S–10°S, 80°E–110°E)
SLP_ENP_MAM	SLP	SLP anomaly over eastern north Pacific (10°N–22.5°N, 160°W–120°W)
VR500_WP_MAM	500 hPa vorticity	500 hPa vorticity over Pacific (0°–10°N, 120°E–160°E)
U500_WPd_MAM	500 hPa U	500 hPa U shear anomaly over Pacific which is the difference between U at (15°N–25°N, 140°E–160°E) and (0°N–10°N, 140°E–170°E)

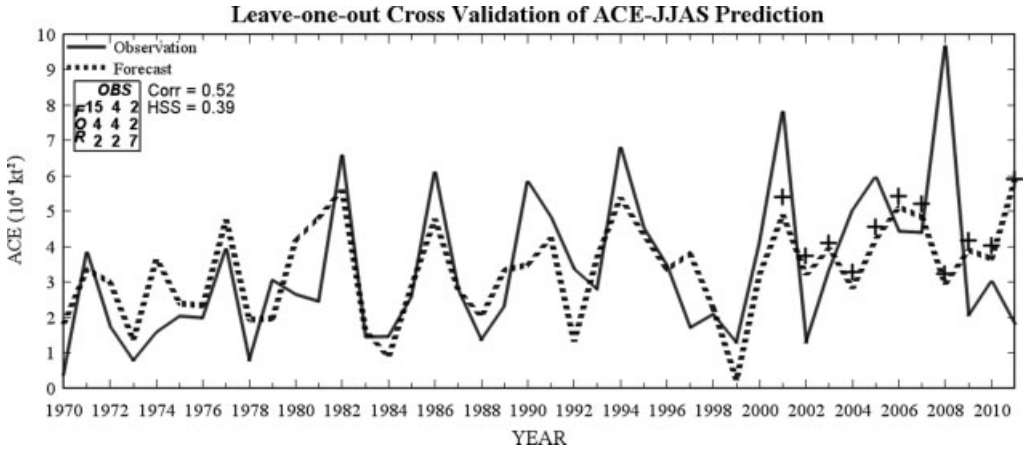

Figure 5. The time series of the leave-one-out cross validation result of the forecast ACE-JJAS (dashed line) compared with the observation (solid line) during the period from 1970 to 2011. The predictors of the forecast model are SST_CIO_05-04, SLP_CN_MAM, SST_SIO_MAM, and SST_WP_MAM. A description of the predictors is summarized in Table 1. On the upper left corner are the correlation (Corr) between two time series, Heidke skill score (HSS) of the forecast model and the 3×3 verification contingency table with forecast (FOR) categories on the rows and observation (OBS) categories on the columns. The retrospective forecast results are marked by '+'.

past decade. The model correctly predicted above normal ACE-JJAS in 2012.

4. Physical basis of the predictability

Any statistical or empirical model is meaningful only if the selected predictors have their own physical meaning. The predictability of the presented statistical forecast models is rooted in the spring-to-summer evolution of the IO-monsoon-ENSO system. The simultaneous correlation maps (Figure 6) between ACE-JJAS and the seasonal (June–September) mean SST, SLP, and 850 hPa winds can be used as a good starting point to explain the relationship. The correlation is based on the data from 1970–2011 but without the extreme year 2008. The ACE-JJAS in 2008 is extremely high (Figure 5) but the large-scale condition is very different from other TC active years. We will discuss this special case in later part of the paper.

4.1. Simultaneous correlation between ACE-JJAS and large-scale environment variable

Figure 6 shows that ACE-JJAS is positively correlated with the SSTs over the central and eastern Pacific within the tropics. The highest correlation appears near 5°S–5°N and 160°E–180°E which is the western part of the Niño

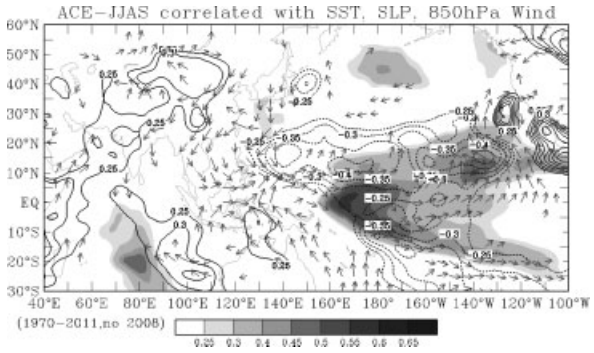

Figure 6. The linear correlation for the period of 1970–2011 (without 2008) between ACE-JJAS and the peak-TC seasonally (JJAS) averaged SLP (contour), SST (shade) and 850-hPa winds. Only correlations significant at the level of 0.05 are presented.

4 area (5°S–5°N and 160°E–150°W). A boomerang-like pattern of positive correlation extended from the equatorial region to the subtropics in both hemispheres around 20°N and 20°S. Corresponding to the positive equatorial Pacific SST anomalies, negative correlations of ACE-JJAS and SLP are found in an east–west zone extending from the Philippine Sea to the eastern Pacific at 120°W. The negative SLP correlation means that the weakening of WNP subtropical high over the Philippine Sea is a critical circulation condition for more TCs affecting Taiwan. The lowering pressure over the Philippine Sea is a consequence of the equatorial western Pacific warming, which, by enhanced convection, can generate ascending atmospheric Rossby waves that enhance the Philippine Sea Low in their westward journey. Therefore, the persistent equatorial western Pacific warming is vital for increased TCs affecting Taiwan. This indicates that the predictor SST_WP_MAM, i.e. the equatorial western Pacific warming in boreal spring, is an important precursor as SST anomalies often persists.

To the west of the negative SLP correlations in both hemispheres, it shows well organized winds correlated with ACE-JJAS. The correlation patterns of the winds over the South China Sea show strong confluence of the northerly winds from the continent of East Asia and the southerly winds from northeastern IO through the maritime continent of Sumatra and Java. Distinct confluent winds are also found east of the Philippines, where the confluence is formed by the northerly winds from the Japan Sea to the Philippine Sea and the southerly winds blowing from the Tasman Sea to the Coral Sea and the Pacific islands. The winds over the East China Sea, surrounded by Japan, Korea, and China, are anticyclonic. This anticyclone can be influential to the tracks of landfall TCs near the East Asian coast. Large correlations appear not only over the Pacific but also over the IO and Asia continent. Positive SST and SLP correlations are observed over the South IO at the longitudes of 70°E–120°E. The Asia continent sees positive correlation of SLP near Mongolia (40°N–50°N, 90°E–110°E) and the correlation centre is surrounded by the anticyclonic winds. Note the connection of the western rim of the cyclonic circulation over the South China Sea and the northerly wind vectors from Mongolia and northeastern China. It suggests a sustaining effect of the westerly winds over the South China Sea by both zonal and meridional pressure gradients over the western Pacific and the Asian–Australia land bridge.

The simultaneous correlations between ACE-JJAS and the large-scale environment variables strongly suggest that TC activities around Taiwan are affected by both tropical and extratropical influences. To the west of 100°E and east of 130°E the coherent ocean and atmosphere perturbations at higher-latitudes are critical factors, while within the longitudinal band of 100°E–130°E the large-scale anomaly patterns in extratropical and tropical atmosphere and oceans and their interactions are the major influential factors for TC activities.

4.2. Spring to summer evolution of monsoon-ENSO system and northwestern Pacific TC activities

The SST variations over the southeast IO (SEIO) in boreal winter and spring were proposed by previous studies as a stronger than ENSO influence to East Asian summer monsoon (Terray *et al.*, 2005; Yoo *et al.*, 2006). SEIO is an area with most active tropical convection during boreal spring. The suppressed convection over SEIO during boreal spring as an atmospheric heat sink may generate descending Rossby waves to the west which can enhance the initial high pressure where the subsidence is generated (Terray *et al.*, 2005; Terray *et al.*, 2007). The anomalous high pressure over the South IO can trigger a wind-thermocline-SST feedback mechanism (Wang *et al.*, 2003; Li *et al.*, 2003) that further suppress convection and cause the anomalous warm SST over the tropical and subtropical South IO and cold SST over eastern IO to the south of Sumatra and northwest of Australia.

The important precursor signal over SEIO is supported by the predictors selected for the forecast model presented in this paper, i.e. SST_SIO_MAM and SST tendency SST_CIO_05-04. More importantly, the selected predictors suggest that in addition to SEIO the mid-latitude perturbations over continental Asia and SST anomalies over the western tropical Pacific are also part of the precursor.

To elaborate this point, we present the lag-correlation maps between ACE-JJAS and the spring season large-scale parameters and mark out the predictors in Figure 7. The correlation is for the period of 1970–2011 without 2008. Over the Asian continent and IO to the west of 110°E, we see significant positive correlation between ACE-JJAS and SLP in the preceding spring season (March–May). To the east of 110°E see large negative correlations over far northeast Asia around the Sea of Japan and the Sea of Okhotsk. Note that the negative correlation over the northeast Asia in Figure 7(a) is much higher than the correlation in Figure 4(b). It suggests an enhanced relationship between ACE-JJAS and the SLP difference between the Asian continent and far northeast

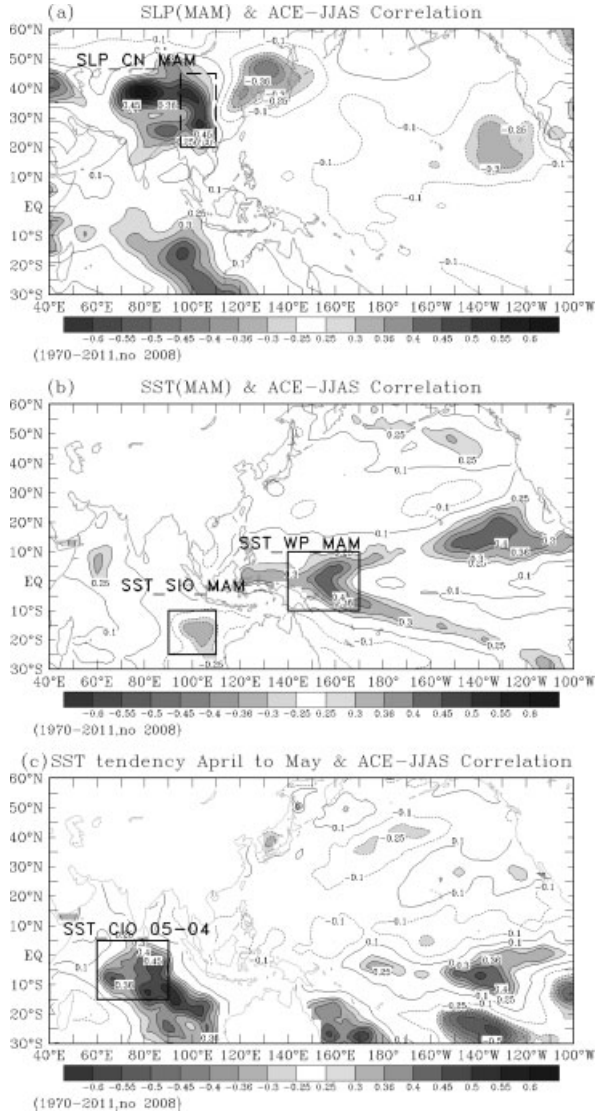

Figure 7. (a) and (b) are the same as Figure 4(a) and (b) but for the period of 1970–2011 (without 2008). The locations of the selected predictors are marked. (c) The linear correlation between ACE-JJAS and the 1-month SST tendency from April to May, with the location of the selected predictor marked. A description of the predictors is summarized in Table 1.

Asia during the warm 2001–2011 decade. The stronger than normal northerly winds over north China associated with the SLP gradient (Figure 6) can be an important precursor for more active TC activity around Taiwan. Figure 7(b) shows significant positive correlation between ACE-JJAS and the SST over the western tropical Pacific, while negative correlation appears over SEIO to the south of Sumatra and northeast of Australia. The SST correlation pattern suggests that a more active typhoon season near Taiwan follows more active convection over western Pacific and suppressed convection over South IO. Comparing Figure 7(b) with Figure 4(a), we find that the favourable condition for more active TC around Taiwan is enhanced after including the past warm decade.

Figure 7(c) shows that the warming tendency of the SSTs over SEIO from April to May is positively correlated with the subsequent typhoon activity near Taiwan. The positive correlation also appears over the marginal seas to the east of Australia and the south east Pacific, which reflects a developing condition of a strong El Niño (Annamalai *et al.*, 2005).

4.3. The 2008 case

2008 is the year with the highest ACE-JJAS in 42 years (Figure 5). However, its large-scale condition is very different from the conditions of other TC active years. The 2008 boreal summer saw a dissipating La Niña episode. The predictors of SST_WP_MAM and SST_CIO_05-04 are usually above normal during the La Niña decaying summer, so were they in 2008, which leads to an above normal forecast ACE-JJAS. The other two predictors SLP_CN_MAM and SST_SIO_MAM were negative and positive, respectively, which leads to a below normal forecast ACE-JJAS. Because the anomalies of the latter two predictors are much larger than the former, the final forecast ACE-JJAS is slightly below normal (Figure 5). Note that the 2008 spring season was very warm. The Northern Hemisphere land temperature in March–May 2008 ranks as the third warmest since 1880 (http://www.ncdc.noaa.gov/sotc/global/2008/5). The large negative SLP_CN_MAM, the most influential predictor, reflected the unusually warm land temperature in the Asian continent.

Although the ACE-JJAS is usually above normal during the La Niña decaying summer, the extremely high ACE-JJAS in 2008 was actually not caused by the common pattern of the monsoon-ENSO evolution (Figure 6). The SST, SLP, and 850 hPa wind anomalies in Figure 8 clearly show that the monsoon trough over East Asia-WNP was rather weak during June–September 2008. The negative SLP anomalies are found mainly over the continent. Over the ocean, we see the enhanced western Pacific subtropical high. The Hovmoller diagrams (not shown) of the large-scale variables indicate that the easterly waves over the Pacific were very active. Figure 8 shows that near the equator the anomalous easterly winds were particularly strong. The invading Taiwan TCs were formed out of the easterly waves and steered by the anomalous western Pacific subtropical high from the ocean to the marginal seas around Taiwan. The atmospheric internal variability such as the easterly waves is beyond the predictability of the statistical model presented in this paper.

5. Summary and conclusion

This study presented a statistical model for predicting the seasonal typhoon ACE around Taiwan. To predict the interannual variability of TC activity over a limited area is extremely challenging. However, the presented model, evaluated by leave-one-out, leave-seven-out, and leave-nine-out cross validation tests, shows substantial

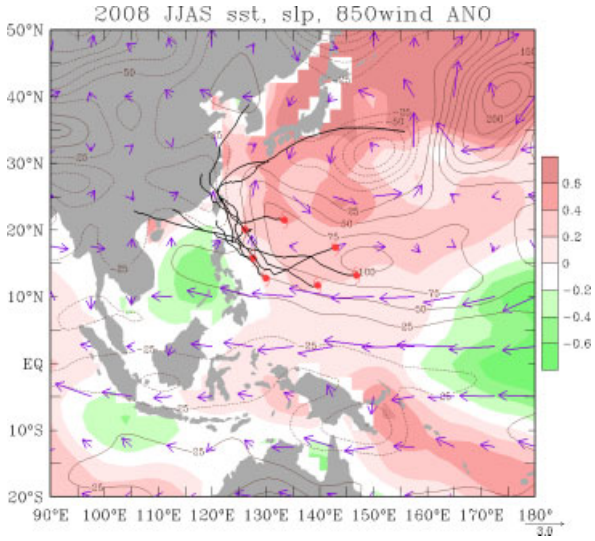

Figure 8. The large-scale parameters of SST (colour), SLP (contours) and 850 hPa wind anomalies. The thick black lines are the tracks of the invading Taiwan TCs and the red marks indicate the first TC records in the best track data. The unit of the SLP is Pa, SST is °C.

forecast skill. The retrospective forecast experiment for 2001–2011 also supports the skill of the forecast model. The predictability is rooted in the spring to summer evolution of the IO-monsoon-ENSO system.

The predictors used in the forecast model are the SSTs and its tendency over the tropical southeast IO and northwest Pacific and the SLP over extratropical East Asia during the spring (March–May) season. These predictors capture the precursors of the TC activities near Taiwan during the subsequent typhoon peak (June–September) season. The typhoon activities near Taiwan are highly correlated with the summer SSTs over South IO and tropical central Pacific, and the SLP and winds associated with the western Pacific monsoon trough.

The physical basis of the forecast model can be understood using the spring to summer evolution framework of the IO SST-monsoon-ENSO system documented by Yoo *et al.* (2006). Affected by the atmospheric tropical waves generated by the heating associated with the IO SST anomalies, the western Pacific monsoon trough tends to be strong (weak) when the south east IO SST is colder (warmer) than normal. The wind-thermocline-SST feedback mechanism (Wang *et al.*, 2003; Li *et al.*, 2003) over the tropical eastern IO, South China Sea, and western Pacific region can be enhanced and sustained by the anomalous meridional winds along the west rim of the Pacific generated by the east–west SLP gradient anomalies over mid-latitude Far East Asia.

While the predictors have clear physical meaning for predicting TCs affecting Taiwan, they are derived from a limited period of observations. The evolution of the IO-monsoon-ENSO system is modulated by longer time scale variability. The nonstationary aspect or the long-term change of the predictor–predictand relationship, which is often seen in empirical prediction, deserves further studies. In addition, the understanding gained here is also useful for establish dynamical–statistical model prediction, which is under investigation.

The ACE-JJAS prediction presented in this paper may have further implications to a region much larger than Taiwan. The correlation between the ACE in this paper and the ACE of TCs in the area of 115°–124°E and 20°–30°N is 0.97. The high correlation is consistent with the ACE map shown in Figure 2, where we see Taiwan is located in a critical location for representing the TC activity north of 20°N and west of 124°E. The application of ACE-JJAS forecasting to areas outside Taiwan need further studies in the future.

Acknowledgements

This study was supported in part by the Central Weather Bureau under the *Hazardous Weather Monitoring and Forecasting Systems Enhancement Project* and the National Science Council of the Republic of China under Grant NSC99-2625-M-052-002-MY3 to Central Weather Bureau. Bin Wang acknowledges support from NASA award (NNX09AG97G).

References

Annamalai H, Xie SP, McCreary JP, Murtugudde R. 2005. Impact of Indian Ocean sea surface temperature on developing El Niño. *Journal of Climate* **18**: 302–319, DOI: 10.1175/JCLI-3268.1

Camargo SJ, Barnston AG, Klotzbach PJ, Landsea CW. 2007a. Seasonal tropical cyclone forecasts. *World Meteorological Organization Bulletin* **56**: 297–307.

Camargo SJ, Robertson AW, Gaffney SJ, Smyth P, Ghil M. 2007b. Cluster analysis of typhoon tracks. Part I: General properties. *Journal of Climate* **20**: 3635–3653, DOI: 10.1175/JCLI4188.1

Camargo SJ, Robertson AW, Gaffney SJ, Smyth P, Ghil M. 2007c. Cluster analysis of typhoon tracks. Part II: Large-scale circulation and ENSO. *Journal of Climate* **20**: 3654–3676, DOI: 10.1175/JCLI4203.1

Chan JC-L. 1985. Tropical cyclone activity in the northwest Pacific in relation to the El Niño/Southern Oscillation phenomenon. *Monthly Weather Review* **113**: 599–606, DOI: 10.1175/1520-0493(1985)113<0599:TCAITN>2.0.CO;2.

Chan JC-L. 2000. Tropical cyclone activity over the western North Pacific associated with El Niño and La Niña events. *Journal of Climate* **13**: 2960–2972, DOI: 10.1175/1520-0442(2000)013<2960:TCAOTW>2.0.CO;2.

Chan JC-L, Shi JS, Lam CM. 1998. Seasonal forecasting of tropical cyclone activity over the western North Pacific and the South China Sea. *Weather and Forecasting* **13**: 997–1004, DOI: 10.1175/1520-0434(1998)013<0997:SFOTCA>2.0.CO;2.

Choi K-S, Kim DW, Byun HR. 2009. Statistical model for seasonal prediction of tropical cyclone frequency around Korea. *Asia-Pacific Journal of Atmospheric Sciences* **45**: 21–32.

Chu JH, Sampson CR, Levine AS, Fukada E. 2002. *The joint typhoon warning center tropical cyclone best-tracks, 1945–2000*. NRL Reference Number: NRL/MR/7540-02-16, http://www.npmoc.navy.mil/jtwc/best_tracks/ TC_bt_report.html.

Chu PS, Zhao X, Lee CT, Lu M-M. 2007. Climate prediction of tropical cyclone activity in the vicinity of Taiwan using the multivariate least absolute deviation regression method. *Terrestrial, Atmospheric and Oceanic Sciences* **18**: 805–825, DOI: 10.3319/TAO.2007.18.4.805(A)

Chu PS, Zhao X, Ho CH, Kim HS, Lu M-M, Kim JH. 2010. Bayesian forecasting of seasonal typhoon activity: A track-pattern-oriented categorization approach. *Journal of Climate* **23**: 6654–6668, DOI: 10.1175/2010JCLI3710.1

DelSole T, Shukla J. 2009. Artificial skill due to predictor screening. *Journal of Climate* **22**: 331–345, DOI: 10.1175/2008JCLI2414.1

Du Y, Yang L, Xie SP. 2011. Tropical Indian Ocean influence on Northwest Pacific tropical cyclones in summer following strong El Niño. *Journal of Climate* **24**: 315–332, DOI: 10.1175/2010JCLI3890.1

Goh AZ-C, Chan JC-L. 2012. Variations and prediction of the annual number of tropical cyclones affecting Korea and Japan. *International Journal of Climatology* **32**: 178–189, DOI: 10.1002/joc.2258

Harr PA, Elsberry RL. 1995. Large-scale circulation variability over the tropical western North Pacific. Part I: Spatial patterns and tropical cyclone characteristics. *Monthly Weather Review* **123**: 1225–1246, DOI: 10.1175/1520-0493(1995)123<1225:LSCVOT>2.0.CO;2.

Ho CH, Baik JJ, Kim JH, Gong DY, Sui CH. 2004. Interdecadal changes in summertime typhoon tracks. *Journal of Climate* **17**: 1767–1776, DOI: 10.1175/1520-0442(2004)017<1767:ICISTT>2.0.CO;2.

Ho CH, Kim JH, Kim HS, Sui CH, Gong DY. 2005. Possible influence of the Antarctic Oscillation on tropical cyclone activity in the western North Pacific. *Journal of Geophysical Research* **110**: D19104, DOI: 10.1029/2005JD005766

Kalnay E, Kanamitsu M, Kistler R, Collins W, Deaven D, Gandin L, Iredell M, Saha S, White G, Woollen J, Zhu Y, Leetmaa A, Reynolds B, Chelliah M, Ebisuzaki W, Higgins W, Janowiak J, Mo KC, Ropelewski C, Wang J, Jenne R, Joseph D. 1996. The NCEP/NCAR 40-Year Reanalysis Project. *Bulletin of the American Meteorological Society* **77**: 437–471, DOI: 10.1175/1520-0477(1996)077<0437:TNYRP>2.0.CO;2.

Kim HS, Ho CH, Chu PS, Kim JH. 2010. Seasonal prediction of summertime tropical cyclone activity over the East China Sea using the least absolute deviation regression and the Poisson regression. *International Journal of Climatology* **30**: 210–219, DOI: 10.1002/joc.1878

Kim H-M, Webster PJ, Curry JA. 2011. Modulation of North Pacific tropical cyclone activity by three phases of ENSO. *Journal of Climate* **24**: 1839–1849, DOI: 10.1175/2010JCLI3939.1

Kim ST, Yu JY, Lu M-M. 2012. The distinct behaviors of Pacific and Indian Ocean warm pool properties on seasonal and interannual time scales. *Journal of Geophysical Research* **117**: D05128, DOI: 10.1029/2011JD016557

Kuo HC, Chen JH, Williams RT, Chang C-P. 2001. Rossby waves in zonally opposing mean flow: behavior in the Northwest Pacific summer monsoon. *Journal of the Atmospheric Sciences* **58**: 1035–1050, DOI: 10.1175/1520-0469(2001)058<1035:RWIZOM>2.0.CO;2.

Li T, Wang B, Chang C-P, Zhang Y-S. 2003. A theory for the Indian Ocean Dipole-Zonal Mode. *Journal of the Atmospheric Sciences* **60**: 2119–2135, DOI: 10.1175/1520-0469(2003)060<2119:ATFTIO>2.0.CO;2.

Liu KS, Chan JC-L. 2002. Synoptic flow patterns associated with small and large tropical cyclones over the western North Pacific. *Monthly Weather Review* **130**: 2134–2142, DOI: 10.1175/1520-0493(2002)130<2134:SFPAWS>2.0.CO;2.

Liu KS, Chan JC-L. 2003. Climatological characteristics and seasonal forecasting of tropical cyclones making landfall along the South China coast. *Monthly Weather Review* **131**: 1650–1662, DOI: 10.1175//2554.1

Liu KS, Chan JC-L. 2010. Interannual variation of Southern Hemisphere tropical cyclone activity and seasonal forecast of tropical cyclone number in the Australian region. *International Journal of Climatology* **32**: 190–202, DOI: 10.1002/joc.2259

Lu M-M, Chu P-S, Lin Y-C. 2010. Seasonal prediction of tropical cyclone activity in the vicinity of Taiwan using the Bayesian multivariate regression method. *Weather and Forecasting* **25**: 1780–1795, DOI: 10.1175/2010WAF2222408.1

Montgomery MT, Farrell BF. 1993. Tropical cyclone formation. *Journal of the Atmospheric Sciences* **50**: 285–310, DOI: 10.1175/1520-0469(1993)050<0285:TCF>2.0.CO;2.

Sadler JC. 1978. Mid-season typhoon development and intensity changes and the tropical upper tropospheric trough. *Monthly Weather Review* **106**: 1137–1152, DOI: 10.1175/1520-0493(1978)106<1137:MSTDAI>2.0.CO;2.

Terray P, Dominiak S, Delecluse P. 2005. Role of the southern Indian Ocean in the transitions of the monsoon–ENSO system during recent decades. *Climate Dynamics* **24**: 169–195, DOI: 10.1007/s00382-004-0480-3

Terray P, Chauvin AF, Douville H. 2007. Impact of southeast Indian Ocean sea surface temperature anomalies on monsoon-ENSO-dipole variability in a coupled ocean-atmosphere model. *Climate Dynamics* **28**: 553–580, DOI: 10.1007/s00382-006-0192-y

Wang B, Chan JC-L. 2002. How strong ENSO events affect tropical storm activity over the western North Pacific. *Journal of Climate* **15**: 1643–1658, DOI: 10.1175/1520-0442(2002)015<1643:HSEEAT>2.0.CO;2.

Wang B, Wu R, Li T. 2003. Atmosphere-warm ocean interaction and its impacts on Asian-Australian monsoon variation. *Journal of Climate* **16**: 1195–1211, DOI: 10.1175/1520-0442(2003)16<1195:AOIAII>2.0.CO;2.

Werner A, Holbrook NJ. 2011. A Bayesian forecast model of Australian region tropical cyclone formation. *Journal of Climate* **24**: 6114–6131.

Wilks DS. 2006. *Statistical Methods in the Atmospheric Sciences.* 2nd edn., Academic Press: New York, 627 pp.

Xie S-P, Hu K-M, Hafner J, Tokinaga H, Du Y, Huang G, Sampe T. 2009. Indian capacitor effect on Indo-western Pacific climate during the summer following El Niño. *Journal of Climate* **22**: 730–747, DOI: 10.1175/2008JCLI2544.1

Yoo SH, Yang S, Ho CH. 2006. Variability of the Indian Ocean sea surface temperature and its impacts on Asian-Australian monsoon climate. *Journal of Geophysical Research* **111**: D03108, DOI: 10.1029/2005JD006001

Zhan R, Wang Y, Lei X. 2011. Contributions of ENSO and East Indian Ocean SSTS to the interannual variability of northwest Pacific tropical cyclone frequency. *Journal of Climate* **24**: 509–521, DOI: 10.1175/2010JCLI3808.1

